Experimental studies of the two-step scheme with an intense radioactive ^{132}Sn beam for next-generation production of very neutron-rich nuclei

H. Suzuki,[1,*] K. Yoshida,[1] N. Fukuda,[1] H. Takeda,[1] Y. Shimizu,[1] D. S. Ahn,[1] T. Sumikama,[1] N. Inabe,[1] T. Komatsubara,[1] H. Sato,[1] Z. Korkulu,[1] K. Kusaka,[1] Y. Yanagisawa,[1] M. Ohtake,[1] H. Ueno,[1] T. Kubo,[1] S. Michimasa,[2] N. Kitamura,[2] K. Kawata,[2] N. Imai,[2] O. B. Tarasov,[3] D. Bazin,[3] J. Nolen,[4] and W. F. Henning[4,5]

[1]*RIKEN Nishina Center, 2-1 Hirosawa Wako, Saitama 351-0198, Japan*

[2]*Center for Nuclear Study, University of Tokyo, 7-3-1 Hongo, Bunkyo, Tokyo 113-0033, Japan*

[3]*National Superconducting Cyclotron Laboratory, Michigan State University, 640 South Shaw Lane, East Lansing, Michigan 48824-1321, USA*

[4]*Physics Division, Argonne National Laboratory, Argonne, Illinois 60439, USA*

[5]*Technische Universität München, D-85748 Garching, Germany*

(Received 28 June 2020; revised 4 November 2020; accepted 17 November 2020; published 18 December 2020)

The study of nuclei in the yet-unexplored, very neutron-rich, mid- to heavy-mass region of the nuclear chart, comprising perhaps half of all nuclei predicted to exist, is leading to new and/or upgraded facilities, as well as to research into the underlying production processes. In the present study, the usefulness of the two-step scheme, an alternate method to produce very neutron-rich nuclei, by a combination of an isotope-separation online (ISOL) system as a first step, and in-beam fragmentation of re-accelerated radioactive isotopes (RIs) as a second step, was investigated with a ^{132}Sn beam. Very neutron-rich RIs around the neutron-rich neutron number $N = 82$ region were produced from the 278-MeV/nucleon ^{132}Sn beam impinging on a 5.97-mm Be target, and their production cross sections were measured. Yields were then estimated for the two-step scheme with the ^{132}Sn beam relative to the ones by a one-step scheme, in-flight fission of a ^{238}U beam, for 1-MW proton and ^{238}U beams at respective RI-beam facilities. This comparison suggests that the two-step scheme with the ^{132}Sn beam provides yields >40-times higher than those with the one-step scheme for the very neutron-rich $N = 82$ region. Moreover, by using various RI beams over the nuclear chart from ISOL, certain kinds of very neutron-rich RIs around the supernova *r*-process path can be produced with greater yields than by the one-step approach.

DOI: 10.1103/PhysRevC.102.064615

I. INTRODUCTION

The properties of nuclei, the many-body system of the strong interaction, have been studied extensively. However, major regions of the nuclear chart, representing perhaps as much as half of the nuclei predicted to exist, is still unknown. Exploration of the unknown areas and the limits of nuclear binding are of considerable interest from points of view of nuclear structure, strong-interaction, and nuclear astrophysics. In particular, the extensive region of the very neutron-rich, mid-mass to heavy nuclei, including those of the astrophysical rapid neutron-capture process (*r* process) path [1], is largely unexplored.

For more than a century now, the nuclear chart has evolved [2]. The evolution began with the discovery of different isotopes for a given chemical element, either in the newly discovered radioactive decays or in mass spectrometry [3]. Nuclear reaction, achieved with alpha particles by Rutherford in 1919 [4], led directly or indirectly to charged-particle accelerators [5,6] in the 1930s. Discovery of fission in 1939 [7,8] led to decay spectroscopy of fission fragments and reactions with neutrons. Accelerators played an increasing role, including nuclear fragmentation with light-ion beams in the late 1940s [9] and the technique of isotope-separation online (ISOL) in the 1960s [10,11]. With higher-energy and, in particular, heavy-ion beams since the 1960s, accelerators took the lead. Heavy-ion fusion has produced nuclei up to the proton drip-line as far as the actinides, and the heaviest chemical elements now known [12,13]. Since the 1980s, in-beam fragmentation [14] of nuclei has led to the production and study of nuclei far from the valley of stability, down to microsecond lifetimes.

The method mostly used today for production of mid-mass neutron-rich radioactive isotopes (RIs) is in-flight fission or fragmentation of a ^{238}U beam [15] (one-step scheme). However, this method is also expected to be limited: Production cross sections for the most neutron-rich nuclei in an isotopic chain have been found to dramatically decrease with each additional neutron ($\leqslant 1/10$). Increases in the ^{238}U-beam intensity are expected by about two orders of magnitude, from the current world maximum of 0.094 pμA (1pμA = 6.24×10^{12} particles/s) at the RI Beam Factory (RIBF) at RIKEN [16–18] to future 8 pμA planned for the new Facility for Rare Isotope Beams (FRIB) [19,20], currently under construction at Michigan State University. The latter

*hsuzuki@ribf.riken.jp

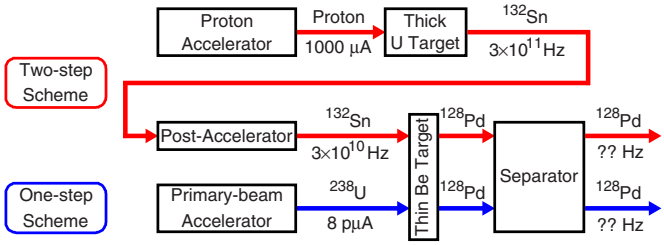

FIG. 1. Flow chart of the two-step and one-step schemes of very neutron-rich radioactive isotope (RI) beams. Cases of ^{128}Pd-beam productions are shown. In the two-step scheme, a long-lived neutron-rich RI (^{132}Sn) is produced by proton-induced spallation, in the first step. Then, it is extracted by ISOL and re-accelerated. In the second step, a more neutron-rich RI beam (^{128}Pd) is produced by projectile fragmentation of ^{132}Sn. In the one-step scheme, ^{128}Pd is produced by in-flight fission of ^{238}U directly.

maximum is close to the 1-MW beam-power limit generally assumed. This has led to considerations for alternative approaches.

As a new method, a two-step scheme [21] has been proposed: A combination of an ISOL system as the first step and in-beam fragmentation as the second step (Fig. 1). In the ISOL part, a high-energy proton beam produces RIs via spallation in a thick ^{238}U target. Higher yields of RIs by several orders of magnitude are achievable, as compared with those from in-flight fission of a ^{238}U beam of equal beam power. However, extraction and re-acceleration of RIs are often severely limited in efficiency and lifetime range. Therefore, the intent is to selectively extract intense thermal-energy beams of longer-lived, easily extractable neutron-rich fission fragments (e.g., ^{132}Sn) and re-accelerate these to the higher energies suitable for fragmentation. In the fragmentation part, cross sections are expected to fall off considerably slower with neutron excess than those for in-flight fission of ^{238}U, as inferred from cases of neutron-rich mid-mass stable nuclei, such as ^{136}Xe [22]. If confirmed, the two-step scheme could open a new window into the unknown region of very neutron-rich mid- to heavy-mass nuclei.

To evaluate the usefulness of the two-step scheme quantitatively, fragmentation cross sections for neutron-rich RI beams need to be studied. A first experiment for the region around the neutron number $N = 82$ shell was performed with a ^{132}Sn beam at GSI [23]. However, the usefulness of the two-step scheme remained unclear, because the study could not reach the very exotic region where the RI yields by the two-step scheme were expected to be larger than those by the in-flight fission of ^{238}U. In the present study, we have been able to measure the cross sections of further neutron-rich RIs from the ^{132}Sn beam. The results show the two-step scheme being more favorable for those nuclei.

Based on our results, we also present a systematic comparison between the yields by the two-step scheme and in-flight fission of ^{238}U for a wide region of the nuclear chart, taking into consideration hypothetical future facilities with 1-MW beam powers. In the calculation of RI-beam production yield, parameters, such as the primary-beam intensities, beam extraction efficiencies, etc., are taken from existing facilities or future facilities under construction or planned for. For the two-step scheme, characteristics of the EURISOL proposal [24] are applied, with a proton beam of 1000-μA intensity and 1-GeV energy (1-MW beam power) plus ISOL extraction efficiencies for RIs as obtained at ISOLDE (CERN) [25–27]. For the one-step approach, i.e., in-flight fission or fragmentation of an intense and high-energy ^{238}U beam, a superconducting heavy-ion linac is used for guidance, such as the one nearing completion at FRIB (8 pμA, 200 MeV/nucleon, and 400 kW; upgradable to 400 MeV/nucleon). For the condition of 1-MW beam power, there are two choices; increasing the beam intensity to 20 pμA or increasing the beam energy to 500 MeV/nucleon. In our comparison, we considered an 8-pμA 500-MeV/nucleon ^{238}U beam, because clean separation between fragments of mid- to heavy-mass elements (atomic number $Z > 40$) would be difficult and complex at 200 MeV/nucleon due to several atomic charge states contributing (similar cases are observed for $Z > 60$ productions at 345 MeV/nucleon at RIBF [28,29]). A beam energy of 500 versus 200 MeV/nucleon results in a small change in cross sections; therefore, we actually use results obtained at

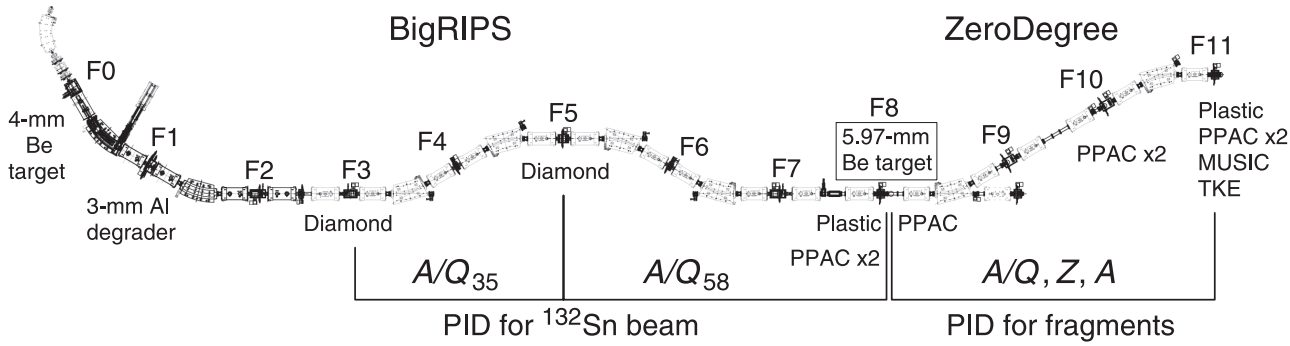

FIG. 2. Schematic of the BigRIPS separator and ZeroDegree spectrometer with targets, degrader, and particle-identification (PID) detectors. The labels Fn indicate foci. The ^{132}Sn beam was separated at the first stage (F0–F2) of BigRIPS and identified at the second stage (F3–F7) and the subsequent F7–F8 matching section by deducing two mass-to-charge ratios (A/Q_{35} and A/Q_{58}). The secondary target of Be was located at F8, the entrance of ZeroDegree. Projectile fragments produced from the ^{132}Sn beam were identified at ZeroDegree by deducing A/Q, Z, and A. See text.

TABLE I. Summary of the experimental conditions for the ^{132}Sn beam in BigRIPS.

Primary beam	≈40-pnA[a] 345-MeV/nucleon ^{238}U
Central particle	^{132}Sn^{50+}
Production target	4-mm Be (740 mg/cm^2)
$B\rho$ after the target	7.5094 Tm
Degrader at F1	3-mm Al
F1 slit opening ($\Delta p/p$)	±6.4 mm (±0.3%)
F2 slit opening	±2 mm
F5 slit opening	±15 mm
F7 slit opening	±35 mm

[a]1 pnA = 6.24 × 10^9 particles/s.

345 MeV/nucleon at RIBF in RIKEN [16,17] for the yield comparison.

II. EXPERIMENT

The production cross sections of the very neutron-rich RIs from the ^{132}Sn beam of 278 MeV/nucleon were measured. In-flight fission of a 40-pnA 345-MeV/nucleon ^{238}U primary beam was used to produce the ^{132}Sn beam by impinging on a 4-mm (740 mg/cm^2) Be target at the focus F0, the entrance of the BigRIPS separator [30–32] + ZeroDegree spectrometer [32] system. Figure 2 illustrates the layout of the full experimental apparatus with targets, energy degrader, and the various detectors used in the present study. It also indicates the combinations of deduced particle parameters for the different separator and spectrometer sections that were used for particle identification (PID) of the ^{132}Sn beam and of its fragments in the succeeding reaction. The isotope separation for ^{132}Sn and its neighboring nuclei were performed by the $B\rho$-ΔE-$B\rho$ ($B\rho$ = magnetic rigidity; ΔE = energy loss) technique at the first stage (F0–F2) of BigRIPS, with a 3-mm Al wedge degrader at the F1 dispersive focus. The momentum window was set to be ±0.3% by the F1 slits.

The particle identification for ^{132}Sn was performed at the second stage (F3–F7) of BigRIPS and the subsequent F7–F8 matching section, based on the TOF-$B\rho$ (TOF = time of flight) measurements. Two mass-to-charge ratios between F3 and F5 (A/Q_{35}) and between F5 and F8 (A/Q_{58}) were deduced from the TOF values and $B\rho$ values by the trajectory reconstruction [33] at the respective sections. PID detectors were changed from the standard configuration in Ref. [33]. First, due to high count rates of ≈100 kHz at the maximum, 200-μm-thick diamond detectors with effective areas of 30-mm squares [34] were used at F3 and F5 to obtain timings and positions, instead of the usual plastic scintillators and parallel plate avalanche counters (PPAC) [35]. Second, the F8 plastic scintillator and PPACs were used instead of those at F7 in order to reduce the amount of material between the PID detectors and the secondary target for the ^{132}Sn fragmentation at the entrance of ZeroDegree. Third, ΔE detectors at F7 were also removed to reduce the materials before the secondary target. Unambiguous PID was possible without the ΔE measurement by the particle separation at the first stage and the precise measurements of A/Q at the second stage following the F7-F8 matching section. Table I summarize the experimental conditions of the ^{132}Sn setting at BigRIPS.

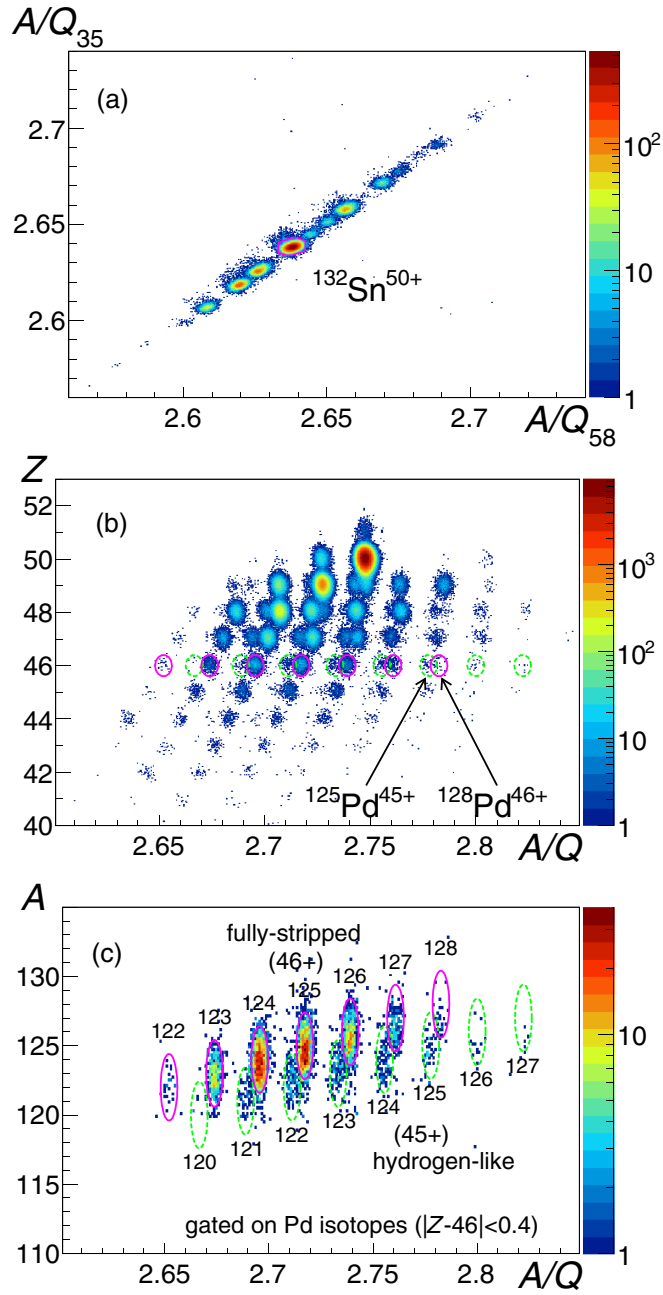

FIG. 3. (a) Correlation plot of A/Q_{35} versus A/Q_{58} for the ^{132}Sn beam in BigRIPS. The subscripts 35 and 58 refer to the A/Q values obtained at F3–F5 and F5–F8, respectively. A gate for the ^{132}Sn^{50+} beam is shown by a solid pink contour. (b) PID plot of Z versus A/Q in ZeroDegree for very neutron-rich RIs produced in the reaction of ^{132}Sn + Be (5.97 mm) at 278 MeV/nucleon obtained in the ^{128}Pd-main setting. Fully stripped and hydrogen-like Pd isotopes are indicated by solid pink contours and dashed lime contours, respectively. The radii of the ellipses are 2.4σ in distribution along each axis. 2.8σ separation was achieved between ^{128}Pd^{46+} and ^{125}Pd^{45+}. (c) A versus A/Q plot of Pd isotopes in the ^{128}Pd-main setting. ≈4σ separation was achieved between fully stripped and hydrogen-like ions.

TABLE II. Summary of the experimental conditions for the cross-section measurements in ZeroDegree.

	^{126}Pd-main setting	^{128}Pd-main setting
Secondary beam	$\approx$ 25-kHz, 278-MeV/nucleon ^{132}Sn	
Central particles of fragments	$^{126}Pd^{46+}$	$^{128}Pd^{46+}$
Secondary target	5.97-mm Be (1100 mg/cm^2)	
$B\rho$ after the target	6.0459 Tm	6.1522 Tm
F9 slit opening ($\Delta p/p$)	$-63.6/+53.0$ mm ($+3/-2.5\%$)	± 63.6 mm ($\pm 3\%$)
F10 slit opening	± 120 mm	± 120 mm
F11 slit opening	± 35 mm	± 35 mm
Dose of ^{132}Sn[a]	4.52×10^8 particles	3.65×10^9 particles
Irradiation time	8.75 hours	69.4 hours

[a]The doses shown are analyzed events in the ^{132}Sn gate. They represent $\approx$ 65% of the incident ^{132}Sn-beam particles due to the dead time of the data acquisition system ($\approx$ 20%) and the efficiencies of the detectors in BigRIPS ($\approx$ 80%).

The correlation plot of A/Q_{35} versus A/Q_{58} is shown in Fig. 3(a). The relative standard-deviation (SD) resolutions were 0.049% and 0.062%, respectively, thus a $\approx 6\sigma$ separation was achieved between ^{132}Sn and the adjacent ^{135}Sb, whose intensity was less than 1/30 of that of ^{132}Sn. The solid pink contour corresponds to a ^{132}Sn gate of $\approx 3.5\sigma$ in radius. Thus, contamination from the neighboring nuclei was negligible. Also, there was no contamination from nuclei with the same A/Q values as ^{132}Sn, such as fully stripped $^{66}Mn^{25+}$ and hydrogen-like $^{132}Sb^{50+}$, because they were removed by the F2 slits. The ^{132}Sn fraction of the beam was $\approx$45%, and its rate was $\approx$25 kHz.

A wide spectrum of fragments, up to $N = 83$, was produced by projectile fragmentation of the ^{132}Sn beam, incident on the secondary target of 5.97-mm Be (1100 mg/cm^2). These RIs were measured by ZeroDegree in four settings: two cross-section measurements (^{126}Pd-main, ^{128}Pd-main) and two background measurements for the ^{126}Pd-main setting. The settings for the two cross-section measurements, summarized in Table II, were for very neutron-rich RIs of $Z = 41$–48, with central particles of ^{126}Pd and ^{128}Pd, respectively. In both settings, the $B\rho$ values were tuned for the corresponding Pd isotopes throughout ZeroDegree. The total doses of ^{132}Sn analyzed in the ^{132}Sn gate were 4.52×10^8 and 3.65×10^9 particles, respectively. The two background settings with a blank target were performed to measure the events from the target holder and the F8 detectors.

PID in ZeroDegree was performed by Z and A/Q based on the TOF-$B\rho$-ΔE method using the plastic scintillators at F8 and F11, the PPACs at F8, F10, and F11, and the ion chamber MUSIC [36,37] at F11, which was the same technique as with the standard PID in BigRIPS [33]. In addition, the total kinetic energy (TKE) was measured with a $LaBr_3$(Ce) crystal of cylindrical shape, with 3-inch diameter, 3-inch length, and covered with a 0.5-mm-thick Al housing [38,39]. It was located the farthest downstream at the F11 focus. The light output from the crystal was read by nine PIN-photodiodes (S3204-08 [40] and S3590-18 [41]) made by Hamamatsu Photonics K.K. The light output was proportional to E^2/Z (E = energy loss in the crystal) due to the quenching effect of the crystal, as shown in Fig. 1 in Ref. [42]. The relative SD E resolution was 0.79% for $\approx$200-MeV/nucleon Pd isotopes. Using TKE and velocity β deduced from TOF, the mass number A was obtained for an additional identification of the RIs.

The PID plot of Z versus A/Q in the ^{128}Pd-main setting is shown in Fig. 3(b). The fully stripped and hydrogen-like Pd isotopes are encircled by solid pink lines and dashed lime lines, respectively. The relative SD A/Q resolution was 0.061%, i.e., 2.8σ separation was achieved in A/Q between, e.g., fully stripped $^{128}Pd^{46+}$ and hydrogen-like $^{125}Pd^{45+}$, located next to each other in the plot. The relative SD Z resolution was 0.37%, thus 5.8σ separation was achieved in Z direction.

The A versus A/Q plots for the Pd isotopes is shown in Fig. 3(c). The A resolution was 0.80%, thus 2.9σ separation was achieved in the A direction between the adjacent nuclei. By a combination of A and A/Q separation, $\approx 4\sigma$ separation was achieved overall. From the A versus A/Q plot of each isotopic line, production yields were deduced. A ratio of the background events to the total events was estimated to be $<1\%$ from the background settings.

The production cross sections were deduced based on the transmission efficiency calculated by the LISE^{++} code [43], in which charge-changing reactions at each material are included. In the simulation, the $B\rho$ values of the dipoles were tuned to reproduce the position distributions of the fragments obtained in the experiment. The needed shifts were of the order of 0.1%.

III. RESULTS

Figure 4 shows the cross sections obtained in the present study together with the earlier results from GSI [23] and predictions of CORFA1.0 [44], a simplified Abrasion-Ablation model, and EPAX3.1a [45], the most-used semiempirical formula. The shapes of the symbols of the data from our present study indicate the ZeroDegree settings. The filled and open symbols indicate that the distribution peaks were located inside and outside the slit opening at the dispersive focus F9, respectively. The data for the same isotope obtained from different settings were consistent with each other, indicating the reliability of our measurements and simulations. From the differences of the cross-section values measured in the two Pd settings, systematic errors caused by the simulation of the transmission were estimated by the method in Ref. [28]. We

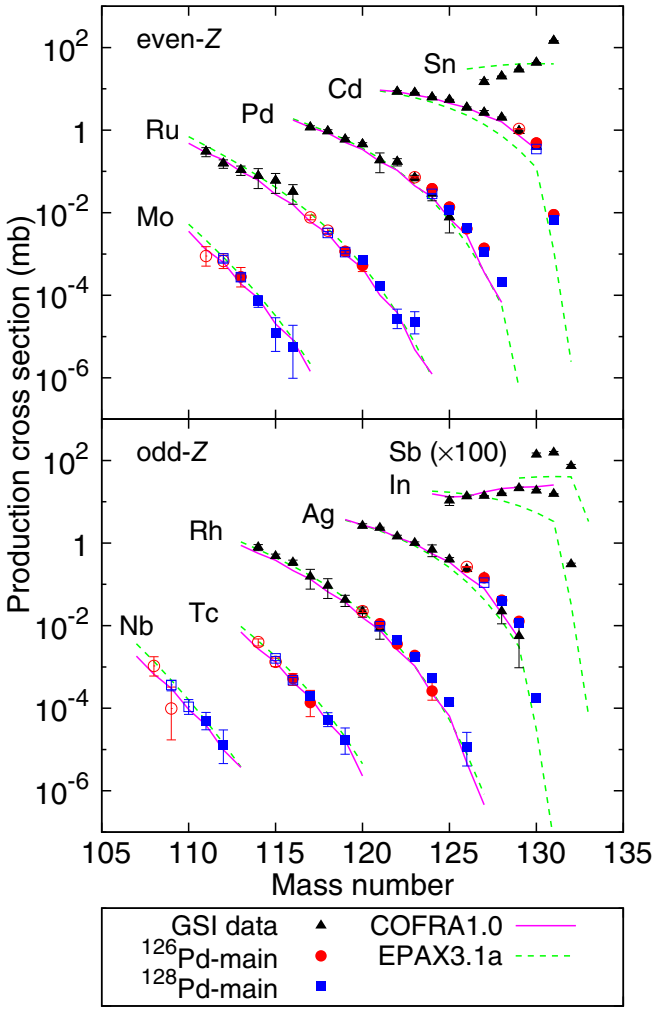

FIG. 4. Measured production cross sections of very neutron-rich RIs produced in the reaction of ^{132}Sn + Be at 278 MeV/nucleon. The red circles and blue squares indicate the RIs produced in the ^{126}Pd-main and ^{128}Pd-main settings, respectively. The filled and open symbols indicate that the distribution peaks were located inside and outside the slit opening at F9, respectively. The black triangles show the data from GSI [23]. The solid pink lines and dashed lime lines show the predictions by the COFRA1.0 [44] and EPAX3.1a [45] codes, respectively. Errors shown are statistical only.

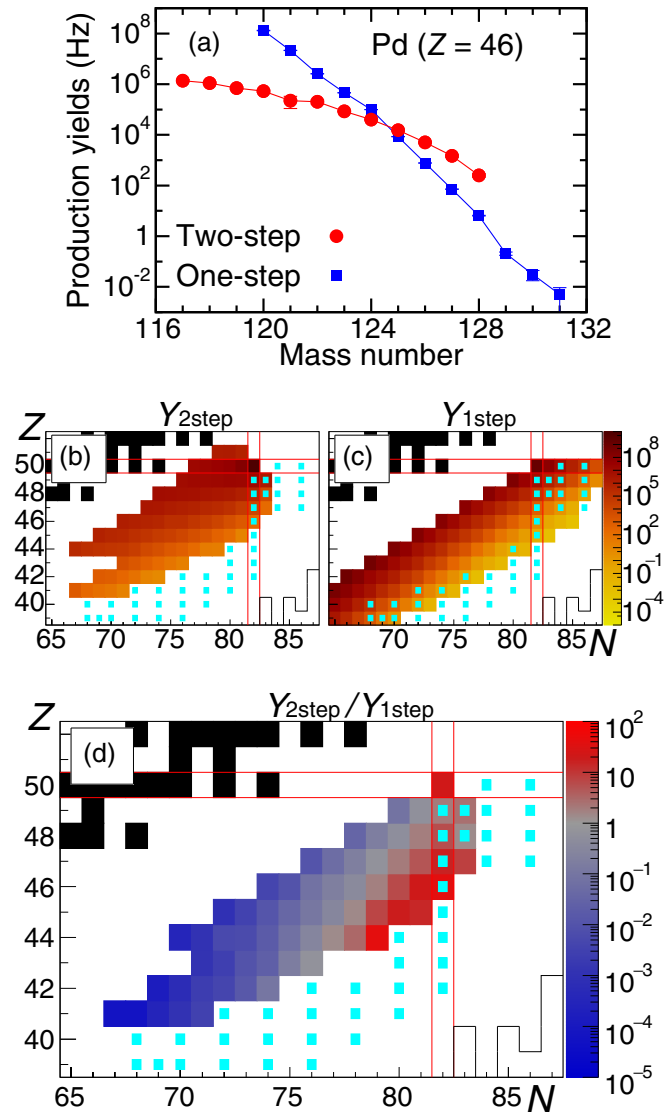

FIG. 5. (a) Yield comparisons between the two-step scheme with a ^{132}Sn beam (red circles) and the one-step in-flight fission of a ^{238}U beam (blue squares) for Pd ($Z = 46$) isotopes. See text for the assumptions of the primary-beam intensities, production targets, and transmissions in a separator. (b) Expected yields by the two-step scheme with a ^{132}Sn beam. The cross-section data are from this work and from GSI [23]. Black squares show stable nuclei. Red lines indicate the magic numbers; ^{132}Sn is located at their cross point. The neutron drip-line predicted by KTUY05 [46] is shown by black lines. The supernova *r*-process path [1] predicted by ETFSI-Q [47] is shown by cyan square dots. (c) Expected yields by the one-step scheme. The cross-section data are from Refs. [48–50] measured at RIKEN. (d) Ratios of the two-step yields in panel (b) to the one-step yields in panel (c). Moving away from the stability line, the ratio systematically increases. It reaches values of ≈40 at ^{128}Pd.

assumed that the systematic error was an averaged value of the square-root of unbiased variances of ratios of the measured cross sections to the averaged one for each nuclide. It was estimated to be ±14%. Both codes reproduce the experimental cross sections well, except the isotopic chains with the highest Z, such as Cd and In, where COFRA1.0 does noticeably better.

IV. DISCUSSION

Based on our measurements, we examine whether and to what extent a two-step approach at future high-power facilities could reach further into the neutron-rich region. As a first case, we compare expected yields between the two-step scheme with the ^{132}Sn beam (Y_{2step}) and one-step in-flight fission of the ^{238}U beam (Y_{1step}), assuming comparable primary-beam power limits.

In the two-step scheme, the parameters for the ISOL driver were taken from the EURISOL proposal (1000 μA) [24]. The beam intensity of ^{132}Sn was estimated to be 3×10^{10} Hz,

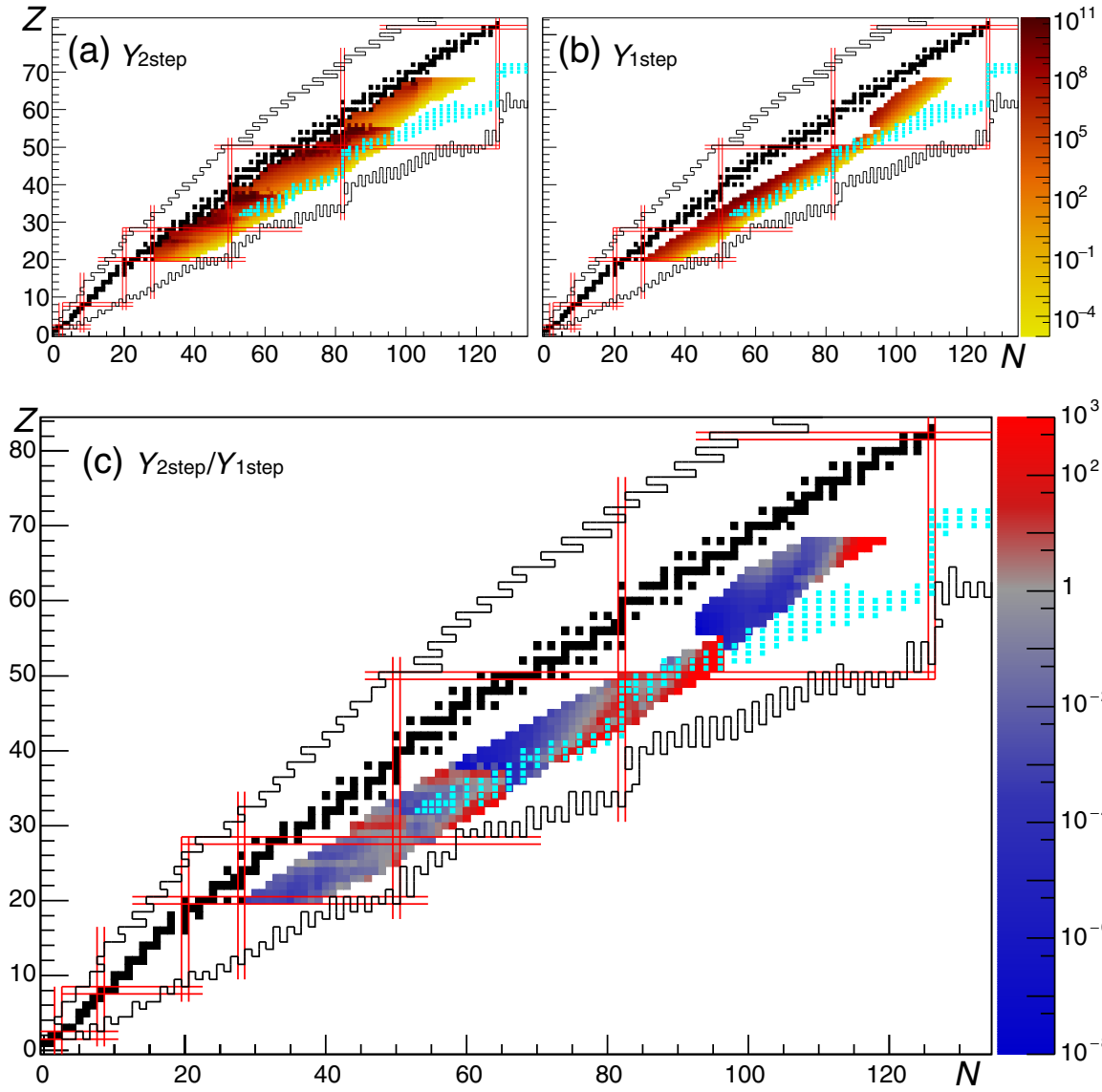

FIG. 6. (a) Expected yields by the two-step scheme with various kinds of RI beams supplied from ISOL. The RI-beam intensities from ISOL are estimated by using the ISOLDE database [27]. The cross-section data are estimated by using the COFRA code [44] with the experimental results from this work and from GSI [23] for the ^{132}Sn beam. See text for other assumptions. The yield of each nuclide (Z_{2step}, N_{2step}) plotted was chosen to be the highest one among all fragment yields produced from heavier RI beams ($Z \geqslant Z_{2step}$, $N \geqslant N_{2step}$) supplied from ISOL. (b) Expected yields by the one-step scheme. The cross-section data are from Ref. [28,48–50,53] measured at RIKEN. For the very exotic regions, where cross sections are not measured yet, we assumed that the cross sections decrease by 1/50 with each added neutron. (c) Ratios of the two-step yields for various kinds of RI beams supplied from ISOL in panel (a) to the one-step yields in panel (b). The two-step scheme is expected to be more useful than the one-step scheme in the very neutron-rich regions around $N = 50$, 60, 82, and 90.

based on an extraction intensity of 3×10^8 Hz/μA from the ISOLDE database [25–27], and a re-acceleration efficiency of 10%. The re-acceleration efficiency was estimated from the beam intensities [18] of ^{238}U, ^{136}Xe, and ^{124}Xe after the RIKEN Ring Cyclotron [51] and after the Superconducting Ring Cyclotron [52] at the RIBF accelerator complex, because the projectile energies need to be accelerated from $\approx$10 MeV/nucleon from the ISOL to relativistic energies ($\gtrsim$300 MeV/nucleon) for projectile fragmentation of nuclei with $Z \approx 50$. The production target for the exotic RIs was chosen to be 4-mm Be. The transmission in a separator was estimated to be 80%, which is the maximum value in BigRIPS for projectile fragmentation. The projectile energy of 500 MeV/nucleon makes fully stripped RIs more than 90% in charge-state distributions, thus we assumed that all fragments were fully stripped in this comparison.

For the simulation of the one-step scheme, the ^{238}U-beam intensity of 8 pμA at the FRIB facility [20] under construction was assumed at a higher beam-energy of 500 MeV/nucleon to reflect 1-MW beam power. The Y_{1step} yields were obtained with a 4-mm Be target and production cross sections from the measurements of ^{238}U + Be at 345 MeV/nucleon at RIBF [48–50]. The transmission was estimated to be 30% from production of $Z \approx 50$ nuclei at BigRIPS.

The comparison between the yields for the Pd isotopes is shown in Fig. 5(a). Y_{2step} decreases more slowly with increasing neutron number than Y_{1step}. Up to ^{124}Pd, Y_{2step} is smaller than Y_{1step}; however, Y_{2step} becomes larger for heavier Pd isotopes beyond ^{124}Pd. At ^{128}Pd, with $N = 82$, Y_{2step} becomes ≈40 times larger than Y_{1step}. Y_{2step} and Y_{1step} for other neutron-rich isotopes are shown in Figs. 5(b) and 5(c), respectively. These figures clearly show that the decrease of Y_{2step} is gentler than that of Y_{1step} with neutron excess. The ratio of Y_{2step}/Y_{1step} for the same area is shown in Fig. 5(d). Moving away from the stability line, the ratio systematically increases. Thus, one might expect the two-step scheme to be more favorable than one-step in-flight fission of a ^{238}U beam also for the increasingly more neutron-rich region beyond our present results, especially for the region of the supernova *r*-process path indicated by cyan square dots in the figures.

The present study has focused on the ^{132}Sn beam which, in the two-step scheme, would be produced as the first step via proton-induced target-spallation + and beam ISOL re-acceleration. This system can provide not only the ^{132}Sn beam but also various other kinds of RI beams over the nuclear chart; thus a wide region of very neutron-rich RIs can in principle be produced by the two-step scheme.

The yield comparison between the two-step scheme with the various kinds of RI beams supplied from ISOL and the one-step scheme with the ^{238}U beam is shown in Fig. 6 for $Z = 20$–68. For the two-step scheme, the ISOLDE database [27] and the COFRA code [44] were used for estimating the RI-beam extraction-intensities from ISOL and their fragment production cross sections, respectively. Y_{2step} of each nuclide (Z_{2step}, N_{2step}) is the highest one among all fragment yields produced from heavier RI beams ($Z \geqslant Z_{2step}, N \geqslant N_{2step}$) supplied by ISOL. Some nuclei, such as ^{132}Sn, can be supplied by ISOL directly without the fragmentation process with the Be target. For the one-step scheme, the cross-section data were obtained from measurements at RIBF [28,48–50,53]. For the very exotic regions, where no cross-section data are available yet, we assumed that the cross sections decrease by 1/50 with neutron number. The beam energy of ^{238}U is assumed to be 500 MeV/nucleon from the beam-power limit of 1 MW. The ratios of fully stripped ions are high enough, >90% for $Z \leqslant 57$, 80% for $Z = 63$, and 70% for $Z = 68$ by the LISE^{++} simulation, thus we assumed that all fragments are fully stripped for simplification. Other assumptions are the same as with the ^{132}Sn-beam case.

Figures 6(a) and 6(b) show the Y_{2step} and Y_{1step} yields, respectively. In both figures, the isotopes are plotted down to 10^{-5} Hz, corresponding to ≈1 event/day. High Y_{2step} yields of isotopes around $Z = 30$, 37, 50, and 55 are obtained due to the high fission in the thick ^{238}U target or high-extraction efficiency of the alkali metals. The ratios of the yields shown in Fig. 6(c) suggest wide regions where the two-step scheme is expected to be more useful than the one-step scheme, i.e., neutron-rich regions around $N = 50$, 60, 82, and 90, including the supernova *r*-process path indicated by cyan square dots. The two-step scheme should be a powerful tool to open a new window into the unknown region of mid-mass to heavy, very neutron-rich nuclei.

V. CONCLUSION

In this paper, we have studied the usefulness of the two-step scheme with a ^{132}Sn beam by comparing with the one-step in-flight fission of a ^{238}U beam for RI-beam production in the neutron-rich $N = 82$ region. Very neutron-rich RIs, including Pd isotopes up to ^{128}Pd, were produced from a 278-MeV/nucleon ^{132}Sn beam impinging on a 5.97-mm (1100 mg/cm^2) Be target, and the production cross sections were measured. The cross sections are well reproduced by the COFRA1.0 code. Yields were then estimated for the two-step scheme with the ^{132}Sn beam relative to those from one-step scheme, for the 1-MW proton and ^{238}U beams expected at hypothetical future RI-beam facilities. This comparison suggests that the two-step scheme with the ^{132}Sn beam provides >40-times higher yields than the one by the one-step scheme in the very neutron-rich $N = 82$ region. Moreover, by using various kinds of RI beams in the nuclear chart from ISOL for the two-step scheme, many very neutron-rich RIs around the supernova *r*-process path can be produced with greater yields than the current method of in-flight fission of ^{238}U. By using the two-step scheme, additional progress in the expansion of the nuclear chart is expected.

ACKNOWLEDGMENTS

The present measurements were carried out at the RI Beam Factory operated by RIKEN Nishina Center, RIKEN, and CNS, University of Tokyo. The authors are grateful to the RIBF accelerator crew for providing the primary beam. Argonne National Laboratory's work was supported by the Office of Nuclear Physics of the U.S. Department of Energy under contract DE AC02 06CH11357.

[1] H. Schatz *et al.*, Astrophys. J. **579**, 626 (2002).
[2] M. Thonnessen, Rep. Prog. Phys. **76**, 056301 (2013).
[3] F. W. Aston, *Mass Spectra and Isotopes*, 2nd ed. (Longmans, Green & Co., New York, 1942).
[4] E. Rutherford, Philos. Mag. **37**, 581 (1919).
[5] J. D. Cockcroft and E. T. S. Walton, Nature (London) **129**, 649 (1932).
[6] R. Widerøe, Arch. Elektrotech. (Berlin) **21**, 387 (1928).
[7] O. Hahn and F. Strassmann, Naturwissenschaften **27**, 11 (1939).
[8] L. Meitner and O. R. Frisch, Nature (London) **143**, 239 (1939).
[9] J. F. Miller *et al.*, Phys. Rev. **80**, 486 (1950).
[10] A. M. Poskanzer *et al.*, Phys. Rev. Lett. **17**, 1271 (1966).
[11] P. G. Hansen *et al.*, Phys. Lett. B **28**, 415 (1969).
[12] Y. T. Oganessian *et al.*, Prog. Theor. Phys. Suppl. **154**, 406 (2004).

[13] Y. T. Oganessian *et al.*, Eur. Phys. J. A **25**, Suppl. 1, 589 (2005).
[14] T. J. M. Symons *et al.*, Phys. Rev. Lett. **42**, 40 (1979).
[15] M. Bernas *et al.*, Phys. Lett. B **331**, 19 (1994).
[16] Y. Yano, Nucl. Instrum. Methods Phys. Res., Sect. B **261**, 1009 (2007).
[17] H. Okuno *et al.*, Prog. Theor. Exp. Phys. **2012**, 03C002 (2012).
[18] Beam intensity of accelerators in RIBF Introduction to RI Beam Factory and User's Information webpage, https://www.nishina.riken.jp/RIBF/accelerator/tecinfo.html.
[19] FRIB web page, https://frib.msu.edu.
[20] M. Hausmann *et al.*, Nucl. Instrum. Methods Phys. Res., Sect. B **317**, 349 (2013).
[21] K. Helariutta *et al.*, Eur. Phys. J. A **17**, 181 (2003).
[22] J. Benlliure *et al.*, Phys. Rev. C **78**, 054605 (2008).
[23] D. Pérez-Loureiro *et al.*, Phys. Lett. B **703**, 552 (2011).
[24] EURISOL web page, https://www.eurisol.org.
[25] S. Lukić *et al.*, Nucl. Instrum. Methods Phys. Res., Sect. A **565**, 784 (2006).
[26] U. Köster *et al.*, Nucl. Instrum. Methods Phys. Res., Sect. B **266**, 4229 (2008).
[27] ISOLDE Yield Database webpage, http://isoyields-classic.web.cern.ch/query_tgt.htm.
[28] N. Fukuda *et al.*, J. Phys. Soc. Jpn. **87**, 014202 (2018).
[29] T. Sumikama *et al.*, Nucl. Instrum. Methods Phys. Res., Sect. B **463**, 237 (2020).
[30] T. Kubo, Nucl. Instrum. Methods Phys. Res., Sect. B **204**, 97 (2003).
[31] T. Kubo *et al.*, IEEE Trans. Appl. Supercond. **17**, 1069 (2007).
[32] T. Kubo *et al.*, Prog. Theor. Exp. Phys. **2012**, 03C003 (2012).
[33] N. Fukuda *et al.*, Nucl. Instrum. Methods Phys. Res., Sect. B **317**, 323 (2013).
[34] S. Michimasa *et al.*, Nucl. Instrum. Methods Phys. Res., Sect. B **317**, 710 (2013).
[35] H. Kumagai *et al.*, Nucl. Instrum. Methods Phys. Res., Sect. B **317**, 717 (2013).
[36] H. Otsu *et al.*, RIKEN Accel. Prog. Rep. **42**, 163 (2009).
[37] Y. Sato *et al.*, Jpn. J. Appl. Phys. **53**, 016401 (2014).
[38] R. Kambayashi, Master's thesis, Rikkyo University, 2011.
[39] K. Kobayashi, Master's thesis, Rikkyo University, 2012.
[40] PIN-photodiodes S3204-08, https://www.hamamatsu.com/jp/en/product/type/S3204-08/index.html.
[41] PIN-photodiodes S3590-18, https://www.hamamatsu.com/jp/en/product/type/S3590-18/index.html.
[42] H. Suzuki *et al.*, RIKEN Accel. Prog. Rep. **52**, 123 (2019).
[43] O. B. Tarasov and D. Bazin, Nucl. Instrum. Methods Phys. Res., Sect. B **266**, 4657 (2008), and references therein; LISE^{++} web page, http://lise.nscl.msu.edu, Michigan State University.
[44] J. Benlliure and K. H. Schmidt, References therein; COFRA web page, http://www.usc.es/genp/cofra, Universidade de Santiago de Compostela.
[45] K. Sümmerer, Phys. Rev. C **86**, 014601 (2012).
[46] H. Koura *et al.*, Prog. Theor. Phys. **113**, 305 (2005).
[47] J. M. Pearson *et al.*, Phys. Lett. B **387**, 455 (1996).
[48] T. Ohnishi *et al.*, J. Phys. Soc. Jpn. **77**, 083201 (2008).
[49] T. Ohnishi *et al.*, J. Phys. Soc. Jpn. **79**, 073201 (2010).
[50] Y. Shimizu *et al.*, J. Phys. Soc. Jpn. **87**, 014203 (2018).
[51] M. Kase *et al.*, Present status of the RIKEN Ring Cyclotron, *Proc. 17th Int. Conf. on Cyclotrons and Their Applications, Tokyo, Japan* (2004), pp. 160–162, http://accelconf.web.cern.ch/AccelConf/c04/data/CYC2004_papers/18P24.pdf.
[52] H. Okuno *et al.*, Magnets for the RIKEN Superconducting Ring Cyclotron, *Proc. 17th Int. Conf. on Cyclotrons and Their Applications, Tokyo, Japan* (2004), pp. 373–377, http://accelconf.web.cern.ch/AccelConf/c04/data/CYC2004_papers/20B1.pdf.
[53] T. Sumikama, S. Nishimura, H. Baba, F. Browne, P. Doornenbal, N. Fukuda, S. Franchoo, G. Gey, N. Inabe, T. Isobe, P. R. John, H. S. Jung, D. Kameda, T. Kubo, Z. Li, G. Lorusso, I. Matea, K. Matsui, P. Morfouace, D. Mengoni *et al.*, Phys. Rev. C **95**, 051601(R) (2017).